www.czasopisma.pan.pl PAN www.journals.pan.pl
Archives of Acoustics Vol. 47, No. 1, pp. 97–112 (2022), doi: 10.24425/aoa.2022.140736

Research Paper

Acoustic Response of an Isotropic Beam Under Axially Variable Loads Using Ritz and Rayleigh Integral Methods

Somi Naidu BALIREDDY(1), Jeyaraj PITCHAIMANI(1)*,
Lenin Babu MAILAN CHINNAPANDI(2), V.S.N. Reddi CHINTAPALLI(3)

(1) *National Institute of Technology Karnataka Surathkal*
Mangalore 575 025, India; e-mail: bnaidus@gmail.com
*Corresponding Author e-mail: pjeyaemkm@gmail.com

(2) *Vellore Institute of Technology Chennai*
Tamilnadu 600 127, India; e-mail: lenin_babu@yahoo.com

(3) *Aditya Engineering College*
Surampalem, Andhra Pradesh, India; e-mail: suryachintapalli@alumni.iitm.ac.in

(*received August 10, 2021; accepted December 20, 2021*)

Vibro-acoustic response of an isotropic beam under the action of variable axial loads (VALs), is presented in the study. Effects of six different types of VALs and three types of end conditions on buckling, free vibration and sound radiation characteristics are investigated. Static buckling and free vibration behaviours using shear and normal deformable theorem and Ritz method. However, the forced vibration response is evaluated using modal superposition method and the acoustic radiation characteristics are obtained using Rayleigh integral. The nature of variation of VALs and end conditions are influencing buckling and free vibration characteristics remarkably. Results indicate that the acoustic response is highly sensitive to the nature of VAL and intensity of the VAL. In general, sound power at resonance decreases when the magnitude of VAL is increased.

Keywords: Ritz method; variable axial load; buckling; vibration; sound radiation.

1. Introduction

Thin-walled beam like structural members are used in automobile, aerospace, marine and nuclear industries. Elastic stability study of these thin-walled beams subjected to compression is very important due to the risk and safety issues. Furthermore, the compressive load also influences dynamic characteristics of the beam. This motivated several researchers to investigate buckling and dynamic characteristics of beams under pre-stress. The changes in dynamic characteristics such as free vibrational frequencies and acoustic response also can be effectively used to analyse the stability of the pre-stressed structural members. Most of the buckling and vibration studies are performed with an assumption of edge compressive load. However, variable axial loads (VAL) along the longitudinal direction is of more practical importance in applications like stiffener of blend wing body aircraft which is subjected to parabolically varying stress in the longitudinal direction (Hu *et al.*, 2003). In general, structure made of an isotropic material is considered first for any type of new investigation. Furthermore, the study based on the isotropic materials gives great motivation for the analysis of structures made of alloys, fibre reinforced composites, functionally graded materials, and other advanced nano composites.

As the current study is focussed on the buckling and dynamic analysis of beam under variable axial load, the related research articles published recently are cited herein. Vo *et al.* (2017) presented normal deformation theory for the analysis of laminated beams. Karamanli and Aydogdu (2019a) analysed buckling of composite beam using Ritz method and reported that nature of VAL affects the buckling load significantly. Karamanli and Aydogdu (2019b) ob-

served that dimensionless fundamental frequencies of laminated composite micro beam is influenced to orthotropy ratios, hub ratios, fiber orientation angels etc. Melaibari *et al.* (2020a) investigated buckling behaviour of sigmoid functionally graded (FG) beam subjected to the VAL using differential quadrature method (DQM) and found that grading of material and nature of the VAL influences the buckling load. Melaibari *et al.* (2020b) analysed stability of a functionally graded beam under the VAL using DQM considering the shear effect and found that the buckling mode shape is influenced by the gradation index. Hamed *et al.* (2020a) carried out numerical study, based on DQM, to analyse buckling characteristics of sandwich beam under the effects of the VAL and elastic foundation. They concluded that the findings will be useful for the design of structural components of aircraft's and ships subjected to the VAL and shear load. Eltaher *et al.* (2020b) used DQM to analyse buckling response of unified composite beams subjected to the VAL and reported that symmetry associated with the buckling mode is altered by the nature of the VAL load. Hamed *et al.* (2020b) performed optimisation study on a porous FG sandwich beam subjected to the VAL using DQM. They reported that nature of porosity variation, porosity coefficient and type of VAL affects the buckling load. Eltaher and Mohamed (2020a) investigated buckling and dynamic response of sandwich beam subjected to VALs and concluded that the analysis is important for the better design of aircraft and naval structural members subjected to nonuniform compressive loads. Abo-bakr *et al.* (2021), using DQM, studied for obtaining optimal weight of functionally graded (FG) in order to improve its buckling strength. Harsha *et al.* (2021) studied effect of graded porosity and nature of variation VAL on buckling and dynamic behaviour of a FG beam using Ritz method. Kanade *et al.* (2021) studied influence of VAL on frequencies of a laminated composite beam using Ritz method and concluded that lamination scheme and nature of variation of the VAL significantly influences the buckling and free vibration characteristics.

For the effective design of a structural component, it is important to predict its static, buckling, and dynamic characteristics accurately. Ritz obtained free vibration characteristics using several admissible functions and minimising a functional involving the total energy (Leissa, 2005). Aydogdu (2005) used Ritz method to analyse frequencies of composites beams under different boundary conditions. Aydogdu (2006) also demonstrated the use of Ritz method to analyse buckling of composite beams by comparing the results with the literature. Jaworski and Dowell (2008) predicted the natural frequencies of a multiple stepped beam using Rayleigh-Ritz formulations, finite element code, and component modal analysis. Zhu (2011) studied on natural frequencies of a pre-twisted beam using Ritz method. Ghannadpour *et al.* (2013) used Ritz method to analyse nonlocal effect on dynamic performance of Euler beams. Ritz method, a numerical method, has been used successfully to analyse the structural mechanics problems (Ilanko *et al.*, 2014) using which combination of trial functions are used to approximate the displacement field. Lord Rayleigh proposed his approach in 1877 to obtain fundamental frequency of beams based on vibration mode shape. Chakraverty and Behera (2015) studied frequencies of nano beams using Ritz method. Nguyen *et al.* (2018) analysed structural behaviour of composite beam for static, buckling, and dynamic characteristics using the Ritz method. Omidi Soroor *et al.* (2021) studied frequencies of magnetorheological fluid sandwich beams based on Ritz method.

Sound radiated from vibrating members is an important problem in order to address the noise control issues arises from structural members during their service. The amount of research work carried out on sound radiation characteristics of beam is very less compared to the plate and cylindrical panels. Vibro-acoustic response studies associated with vibrating beam are presented here. Zheng and Cai (2004) reduced acoustic response from a beam using optimized constrained layer damping method. They used Rayleigh integral to obtain the sound power radiated from the vibrating beam under steady state harmonic excitation. Ruzzene (2004) investigated vibro-acoustic response characteristics of truss core sandwich beam using analytical method. Spadoni and Ruzzene (2006) investigated vibro-acoustic response of chiral truss core sandwich beam using finite element method and Rayleigh integral. Majkut (2006) studied acoustic diagnostics on crack detection of structural element of a CF beam. Denli and Sun (2007) performed optimisation study to minimise the sound power radiation of a cellular core sandwich beam. They used finite element based numerical method to obtain the vibration response and Rayleigh integral to obtain the sound power response. Alshabatat and Naghshineh (2014) worked on optimization of sound power and fundamental frequencies of FG beams by numerical methods. They used finite element method to obtain vibration parameters and Rayleigh integral for the acoustic response evaluation. Tang and Xu (2017) analysed sound radiation of a beam in subsonic flow using theoretical models. They used an analytical method for the structural analysis and Helmholtz equation based theoretical model for the sound radiation analysis.

An experimental procedure for beam type structures was proposed by Torres-Romero *et al.* (2018) for vibro-acoustic studies. Tiryakioglu and Demir (2019) studied on radiation of sound waves from semi-infinite circular cylindrical duct using modified Wiener-Hopf solution. Continuation study on the above circular cylindrical duct was carried by

Tiryakioglu (2020). He used perforated end and with outer wall coated with acoustically absorbent material. Li and Yang (2020) studied sound radiation behaviour of cellular structures with metamaterials. They used Euler-Bernoulli theorem based analytical model to study the vibration response and Rayleigh's first integral to study the sound radiation response. Recently, Gunasekaran and co-authors analysed the influence of nonuniform load on sound radiation of metal (Gunasekaran *et al.*, 2020a), porous grapheme nano composite (Gunasekaran *et al.*, 2020b), and FG grapheme composite (Gunasekaran *et al.*, 2021) plates and highlighted the importance of studying the effect of varying edge load on the vibro-acoustic response.

From the literature, it is evident that it is important to analyse stability and dynamic behaviour of beams subjected to varying load along the longitudinal direction. For example, the stiffeners used to connect different panels in aircraft structures may be subjected to nonuniform shear forces. These members are subjected to steady state mechanical excitation also, due to the engine vibration, apart from the axially varying in-plane loads. However, most of the dynamic response studies are performed with an assumption of compression load applied at the ends of the beam. Furthermore, there is no study available in open literature related to vibro-acoustics of beams under pre-stress and subjected to a harmonic excited mechanical load. The present study analyses vibro-acoustic response of an isotropic beam subjected to VALs under the action of a steady state mechanical load excitation. Ritz method is used to study the buckling and free vibration parameters while Rayleigh integral is used to study the acoustic response parameters.

2. Methodology

The schematic diagram of the studied problem is given in Fig. 1. The beam is studied for simply supported (SS), clamped clamped (CC), and clamped free (CF) boundary conditions. As shown in Fig. 2, six different types of VAL's are considered to analyse the effect of nature of axial load variation along the length

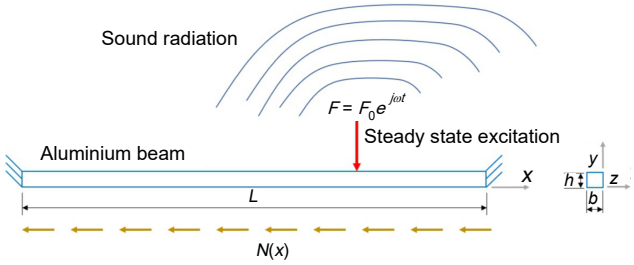

Fig. 1. Schematic diagram of proposed work ($N(x)$ is variable axial load).

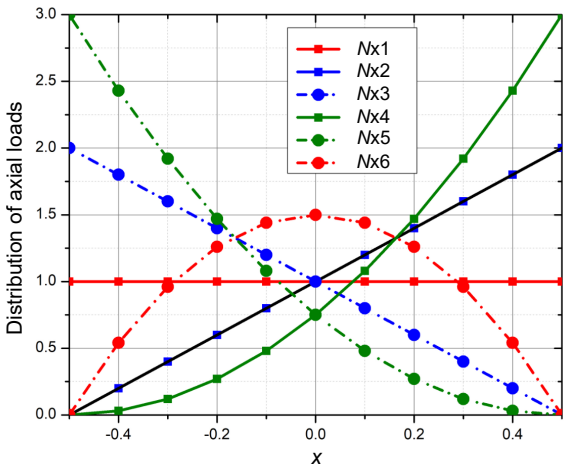

Fig. 2. Distribution of the VALs along the length of the beam (Karamanli, Aydogdu, 2019a).

for the vibro-acoustic response of the beam. The variation of the in-plane loads along the length is defined by the following expression

$$N_x^e(x) = N_0\left\{\beta_1\left(x+\frac{L}{2}\right)^2+\beta_2\left(x+\frac{L}{2}\right)+\beta_3\right\},$$
$$N_x^e(x) = N_0 P(x). \tag{1}$$

The values of β_1, β_2, and β_3 used in Eq. (1) will define the type of VAL and their respective values are given in Table 1. The displacement field based on shear and normal deformable theory is considered (Karamanli, 2019a; 2019b; Nguyen, 2018; Vo, 2017)

$$\begin{aligned} U(x,z,t) &= u(x,t) - z\frac{\mathrm{d}w_b(x,t)}{\mathrm{d}x} - \frac{4z^3}{3h^2}\frac{\mathrm{d}w_s(x,t)}{\mathrm{d}x} \\ &= u(x,t) - zw_b'(x,t) - f(z)w_s'(x,t), \\ W(x,z,t) &= w_b(x,t) + w_s(x,t) + \left(1-\frac{4z^2}{h^2}\right)w_z(x,t) \\ &= w_b(x,t) + w_s(x,t) + g(z)w_z(x,t), \end{aligned} \tag{2}$$

where u is axial displacement, w_b and w_s are components of bending and shear displacements, and w_z is

Table 1. Axial distributed loads coefficients.

Type of loading	Category of loading	β_1	β_2	β_3
N_x^1	Uniformly distributed load	0	0	1
N_x^2	Gradually increasing load	0	2	0
N_x^3	Gradually decreasing load	0	−2	2
N_x^4	Exponentially increasing load	3	0	0
N_x^5	Exponentially decreasing load	3	−6	3
N_x^6	Parabolic load	−6	6	0

accounts for normal deformation effect. The strains of the axial, normal, and shear are described by:

$$\varepsilon_{xx} = \frac{\partial U}{\partial x} = u - zw_b'' - f(z)w_s'',$$
$$\varepsilon_{zz} = \frac{\partial W}{\partial z} = g'(z), \tag{3}$$
$$\gamma_{xz} = \frac{\partial W}{\partial x} + \frac{\partial U}{\partial z} = g(z)(w_s' + w_z').$$

The potential energy is given as

$$U = \frac{1}{2}\int_v (\sigma_{xx}\varepsilon_{xx} + \sigma_{zz}\varepsilon_{zz} + \sigma_{xz}\gamma_{xz})\,\mathrm{d}V. \tag{4}$$

Work done by VAL is

$$V = -\frac{1}{2}\int_{-\frac{L}{2}}^{\frac{L}{2}} N_x^e(x) \cdot\left\{\int_{-\frac{L}{2}}^{x}\left[\left(\frac{\partial w_b}{\partial x}\right)^2 + 2\frac{\partial w_b}{\partial x}\frac{\partial w_s}{\partial x} + \left(\frac{\partial w_s}{\partial x}\right)^2\right]\mathrm{d}x\right\}\mathrm{d}x. \tag{5}$$

The kinetic energy of the system is

$$K = -\int_0^L\int_0^b\left[\int_{\frac{-h}{2}}^{\frac{h}{2}}\rho\left(\dot{U}\delta\dot{U} + \dot{W}\delta\dot{W}\right)\mathrm{d}z\right]\mathrm{d}y\,\mathrm{d}x$$
$$= \int_0^L\Big[\delta\dot{u}(m_0\dot{u} - m_1\dot{w}_b' - m_f\dot{w}_s') + \delta\dot{w}_b[m_0(\dot{w}_b + \dot{w}_s) + m_g\dot{w}_z] + \delta\dot{w}_b'(-m_1\dot{u} + m_2\dot{w}_b' + m_{fz}\dot{w}_s') + \delta\dot{w}_s[m_0(\dot{w}_b + \dot{w}_s) + m_g\dot{w}_z] + \delta\dot{w}_s'(-m_f\dot{u} + m_{fz}\dot{w}_b' + m_{f^2}\dot{w}_s') + \delta\dot{w}_z[m_g(\dot{w}_b + \dot{w}_s) + m_{g^2}\dot{w}_z]\Big]\mathrm{d}x, \tag{6}$$

where

$$(m_0, m_1, m_2) = \int_{\frac{-h}{2}}^{\frac{h}{2}}\rho(1, z, z^2)b\,\mathrm{d}z,$$
$$(m_f, m_{fz}, m_{f^2}) = \int_{\frac{-h}{2}}^{\frac{h}{2}}\rho(f, fz, f^2)b\,\mathrm{d}z, \tag{7}$$
$$(m_g, m_{g^2}) = \int_{\frac{-h}{2}}^{\frac{h}{2}}\rho(g, g^2)b\,\mathrm{d}z.$$

Total potential energy is

$$\Pi = U + V - K. \tag{8}$$

or

$$0 = \int_{t_1}^{t_2}(K - U - V)\,\mathrm{d}t,$$

$$0 = \Bigg[\int_{t_1}^{t_2}\int_0^L\Big[\delta\dot{u}(m_0\dot{u} - m_1\dot{w}_b' - m_f\dot{w}_s') + \delta\dot{w}_b[m_0(\dot{w}_b + \dot{w}_s) + m_g\dot{w}_z] + \delta\dot{w}_b'(-m_1\dot{u} + m_2\dot{w}_b' + m_{fz}\dot{w}_s') + \delta\dot{w}_s[m_0(\dot{w}_b + \dot{w}_s) + m_g\dot{w}_z] + \delta\dot{w}_s'(-m_f\dot{u} + m_{fz}\dot{w}_b' + m_{f^2}\dot{w}_s') + \delta\dot{w}_z[m_g(\dot{w}_b + \dot{w}_s) + m_{g^2}\dot{w}_z]\Big]\mathrm{d}x$$
$$- \frac{1}{2}\int_{-\frac{L}{2}}^{\frac{L}{2}}\Bigg\{A\left(\frac{\partial u}{\partial x}\right)^2 + D\left(\frac{\partial^2 w_b}{\partial x^2}\right)^2 + D_s\left(\frac{\partial^2 w_s}{\partial x^2}\right)^2 + 2H\left(\frac{\partial^2 w_b}{\partial x^2}\right)^2\left(\frac{\partial^2 w_s}{\partial x^2}\right)^2 - 2B\left(\frac{\partial u}{\partial x}\right)\left(\frac{\partial w_b}{\partial x^2}\right)^2 - 2B_s\left(\frac{\partial u}{\partial x}\right)\left(\frac{\partial^2 w_s}{\partial x^2}\right) + 2X\left(\frac{\partial u}{\partial x}\right)w_z - 2Y\left(\frac{\partial^2 w_b}{\partial x^2}\right)w_z - 2Y_s\left(\frac{\partial^2 w_s}{\partial x^2}\right) + Zw_z^2 + A_s\left[\left(\frac{\partial w_s}{\partial x}\right)^2 + \left(\frac{\partial w_z}{\partial x}\right)^2 + 2\left(\frac{\partial w_s}{\partial x}\right)\left(\frac{\partial w_z}{\partial x}\right)\right] - N_0P(x)\Bigg[\int_{\frac{L}{2}}^{x}\Bigg[\left(\frac{\partial w_s}{\partial x}\right)^2 + 2\left(\frac{\partial w_s}{\partial x}\right)\left(\frac{\partial w_z}{\partial x}\right) + \left(\frac{\partial w_z}{\partial x}\right)^2\Bigg]\mathrm{d}x\Bigg]\Bigg\}\mathrm{d}x\,\mathrm{d}t\Bigg]. \tag{9}$$

The stiffness coefficients are

$$(A, B, B_s, D, D_s, H) = \int_{-\frac{h}{2}}^{\frac{h}{2}}Q_{11}b\,(1, z, f, z^2, f^2, fz, g'^2)\mathrm{d}z, \tag{10}_1$$
$$A_s = \int_{-\frac{h}{2}}^{\frac{h}{2}}Q_{55}g^2\,\mathrm{d}z, \tag{10}_2$$

$$(X, Y, Y_s) = \int_{-\frac{h}{2}}^{\frac{h}{2}} Q_{13} b g'\big(1, z, f\big)\,\mathrm{d}z, \tag{10}_3$$

$$Z = \int_{-\frac{h}{2}}^{\frac{h}{2}} Q_{33} b g'^{2}\,\mathrm{d}z. \tag{10}_4$$

For isotropic lamina,

$$Q_{11} = Q_{22} = \frac{E}{1-\nu^2}, \qquad Q_{12} = Q_{21} = \frac{\nu E}{1-\nu^2}, \qquad Q_{33} = Q_{44} = Q_{55} = G. \tag{11}$$

The kinematic relations associated with the SS and CC boundary conditions are shown in Table 2. The functions $u(x,t)$, $w_b(x,t)$, $w_s(x,t)$, and $w_z(x)$ are given as (Karamanli, Aydogdu, 2019a):

$$u(x,t) = \sum_{j=1}^{m} A_j \Theta_j(x) e^{i\omega t}, \qquad \Theta_j(x) = \left(x + \frac{L}{2}\right)^{p_u} \left(x - \frac{L}{2}\right)^{q_u} x^{j-1}, \tag{12}_1$$

$$w_b(x,t) = \sum_{j=1}^{m} B_j \varphi_j(x) e^{i\omega t}, \qquad \varphi_j(x) = \left(x + \frac{L}{2}\right)^{p_{w_b}} \left(x - \frac{L}{2}\right)^{q_{w_b}} x^{j-1}, \tag{12}_2$$

$$w_s(x,t) = \sum_{j=1}^{m} C_j \zeta_j(x) e^{i\omega t}, \qquad \zeta_j(x) = \left(x + \frac{L}{2}\right)^{p_{w_s}} \left(x - \frac{L}{2}\right)^{q_{w_s}} x^{j-1}, \tag{12}_3$$

$$w_z(x,t) = \sum_{j=1}^{m} D_j \psi_j(x) e^{i\omega t}, \qquad \psi_j(x) = \left(x + \frac{L}{2}\right)^{p_{w_z}} \left(x - \frac{L}{2}\right)^{q_{w_z}} x^{j-1}. \tag{12}_4$$

Table 2. Boundary exponents of SS and CC boundary conditions.

BC	Left end				Right end			
	p_u	p_{wb}	p_{ws}	p_{wz}	q_u	q_{wb}	q_{ws}	q_{wz}
SS	1	1	1	1	0	1	1	1
CC	1	2	2	1	1	2	2	1
CF	1	2	2	1	1	2	2	1

In Eq. (12), A_j, B_j, C_j, and D_j are unknown coefficients, $\Theta_j(x)$, $\varphi(x)$, $\zeta_j(x)$, and $\psi_j(x)$ are trial functions and p_ξ and q_ξ are the boundary exponents. The boundary exponents are $\xi = u, w_b, w_s, w_z$.

By using the minimum energy principle and substituting Eqs (12) into Eq. (10), the following eigenvalue problem is obtained (neglecting the inertia terms)

$$\big([K] - N_0[S]\big)\{\Delta\} = 0,$$

$$\left(\begin{bmatrix} [K_{11}] & [K_{12}] & [K_{13}] & [K_{14}] \\ [K_{12}]^{\mathrm{T}} & [K_{22}] & [K_{23}] & [K_{24}] \\ [K_{13}]^{\mathrm{T}} & [K_{23}]^{\mathrm{T}} & [K_{33}] & [K_{34}] \\ [K_{14}]^{\mathrm{T}} & [K_{24}]^{\mathrm{T}} & [K_{34}]^{\mathrm{T}} & [K_{44}] \end{bmatrix} - N_0 \begin{bmatrix} [0] & [0] & [0] & [0] \\ [0] & [S_{22}] & [S_{23}] & [0] \\ [0] & [S_{23}]^{\mathrm{T}} & [S_{33}] & [0] \\ [0] & [0] & [0] & [0] \end{bmatrix}\right) \begin{Bmatrix} \{A\} \\ \{B\} \\ \{C\} \\ \{D\} \end{Bmatrix} = \begin{Bmatrix} \{0\} \\ \{0\} \\ \{0\} \\ \{0\} \end{Bmatrix}, \tag{13}$$

where $'\lambda'$ is dimensionless critical buckling load, $[K]$ and $[S]$ are stiffness and geometric matrices, respectively. The dimensionless critical buckling load can be defined by:

$$\lambda = \frac{N_0 * L^2}{E_1 * b * h^3}. \tag{14}$$

Critical buckling load of the beam under six different VALs is obtained first. Then, free vibration frequencies of beam subjected to VALs are calculated considering the pre-stress effect caused by the in-plane load. The Rayleigh-Ritz method formulated based on the shear and normal deformable theorem is used to investigate static stability and free vibration characteristics. The free vibration is analysed with:

$$\big([K - S] - \omega^2[M]\big)\{\Delta\} = 0,$$

$$\left(\begin{bmatrix} [K_{11}] & [K_{12}] & [K_{13}] & [K_{14}] \\ [K_{12}]^{\mathrm{T}} & [K_{22} - S_{22}] & [K_{23} - S_{23}] & [K_{24}] \\ [K_{13}]^{\mathrm{T}} & [K_{23} - S_{23}]^{\mathrm{T}} & [K_{33} - S_{33}] & [K_{34}] \\ [K_{14}]^{\mathrm{T}} & [K_{24}]^{\mathrm{T}} & [K_{34}]^{\mathrm{T}} & [K_{44}] \end{bmatrix} - \omega^2 \begin{bmatrix} [M_{11}] & [M_{12}] & [M_{13}] & [0] \\ [M_{12}]^{\mathrm{T}} & [M_{22}] & [M_{23}] & [M_{24}] \\ [M_{13}]^{\mathrm{T}} & [M_{23}]^{\mathrm{T}} & [M_{33}] & [M_{34}] \\ [0] & [M_{24}]^{\mathrm{T}} & [M_{34}]^{\mathrm{T}} & [M_{44}] \end{bmatrix}\right) \begin{Bmatrix} \{A\} \\ \{B\} \\ \{C\} \\ \{D\} \end{Bmatrix} = \begin{Bmatrix} \{0\} \\ \{0\} \\ \{0\} \\ \{0\} \end{Bmatrix}, \tag{15}$$

where $[M]$ is the mass matrix, and its coefficients are defined in Appendix.

Followed by this forced vibration, response is evaluated using the modal superposition method:

$$[M]\{\ddot{\Delta}\} + [C]\{\dot{\Delta}\} + [K]\{\Delta\} = [H]e^{j\omega t}. \tag{16}$$

In the above equation, $[C]$ is damping matrix, Δ is displacement, and $[H]$ is harmonic load vector.

The Rayleigh integral (Gunasekaran *et al.*, 2020a) is used in determining the acoustic radiation behaviour of the beam:

$$p(r) = \frac{j\omega\rho_0}{2\pi} \int_S \dot{W}(r_s) \frac{e^{-jk|r-r_s|}}{|r-r_s|}\,\mathrm{d}s, \tag{17}$$

here $p(r)$ is pressure, $\omega(r)$ is surface velocity, k wave number, ρ_0 is fluid density, and $|r - r_s|$ represents for the distance among the surface and field. The sound intensity is

$$I(r) = \frac{1}{2}\mathrm{Re}\left(p(r)\dot{w}^*(r_s)\right), \tag{18}$$

and the sound power radiated is

$$\overline{W} = \oint I(r)\, n(r_s)\, \mathrm{d}s, \tag{19}$$

here $n(r_s)$ is surface normal

$$\overline{W} = \frac{1}{2}\mathrm{Re}\left(\oint p(r)\dot{W}^*(r)\, \mathrm{d}s\right). \tag{20}$$

From the above equation, the sound power level (SWL) of an isotropic beam can be determined by solving Eq. (21):

$$\mathrm{SWL} = 10 \log \frac{\overline{W}}{W_{\mathrm{ref}}}, \tag{21}$$

where W_{ref} is reference sound power level, which is 10^{-12} W, and the sound radiation efficiency (σ) can be obtained from the following formula:

$$\sigma = \frac{\overline{W}}{\rho_0 C_0 S \left\langle \overline{\dot{W}}^2 \right\rangle}. \tag{22}$$

In the above equation, C_0 is speed of sound in m/s, $\left\langle \overline{\dot{W}}^2 \right\rangle = \dot{W}_n^H N \dot{W}_n$, and $N = (1/2)NI$. 'I' is a unit matrix in a respective size, N is elements number used in discretization, $\dot{W}_n$ and $\dot{W}_n^H$ represents normal velocity with its conjugate velocity.

3. Validation study

The present study on isotropic beams is validated with earlier studies.

3.1. Buckling load calculation

The present study is validated for buckling load by considering isotropic beam analysed by Karamanli and Aydogdu (2019a). Both Karamanli and Aydogdu (2019a) present methods used the same theorem and the Ritz method to evaluate the nondimensional buckling load (λ) of Eq. (14). The isotropic beam with length 1 m, cross section $b \times h$ assumed to be square and for L/h ratio of 50 is used for the comparison. The results of nondimensional buckling load obtained using present study are presented along with results of Karamanli and Aydogdu (2019a) in Table 3. The percentage in error in Table 3 is found to be considerably less.

3.2. Natural frequency sound radiation calculation

The present study is also validated for SWL calculation of an isotropic beam studied by Zheng and Cai (2004). Aluminium beam with $0.4 \times 0.03 \times 0.004$ m^3 under SS boundary condition is considered for comparison. Zheng and Cai (2004) used Rayleigh's integral in calculating the sound power level. The sound power responses calculated using the present approach are compared with Zheng and Cai (2004) in Fig. 3.

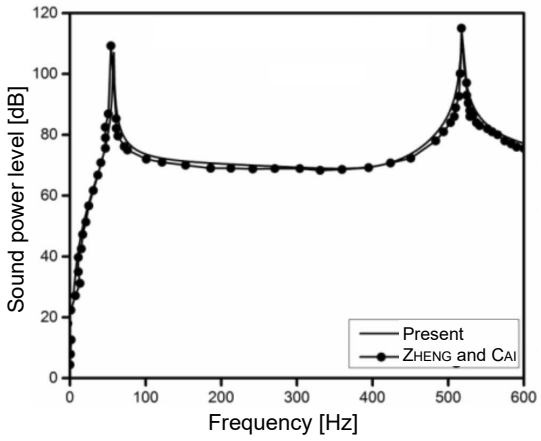

Fig. 3. Comparison of natural frequency and SWL with (Zheng, Cai, 2004).

Table 3. Comparison of buckling loads calculated using present method with Karamanli and Aydogdu (2019a) results.

BC	Study	N_x^1	N_x^2	N_x^3	N_x^4	N_x^5	N_x^6
SS	Karamanli and Aydogdu (2019a)	18.55	15.34	23.21	14.14	26.64	18.33
	Present study	18.76	15.51	23.47	14.30	26.94	18.53
	Absolute error [%]	1.11	1.10	1.12	1.10	1.13	1.11
CC	Karamanli and Aydogdu (2019a)	74.59	56.23	107.78	50.21	139.50	72.68
	Present study	75.42	56.86	108.97	50.77	141.04	73.51
	Absolute error [%]	1.11	1.12	1.11	1.12	1.10	1.13
CF	Karamanli and Aydogdu (2019a)	7.85	5.13	16.14	4.23	27.35	8.73
	Present study	7.92	5.18	16.27	4.27	27.55	8.80
	Absolute error [%]	0.84	0.85	0.79	0.86	0.74	0.82

From all the comparison studies, it is very clear that the present study can be extended for the analysis that are discussed earlier.

4. Results and discussion

The vibro-acoustic response of an isotropic beam under various VALs, and boundary conditions is investigated in this section. The study is presented for six types of VALs and under SS, CC, and CF end conditions. To start with, the buckling loads are calculated first for each boundary condition under different VALs and the same are tabulated in Table 4 and plotted in Fig. 4. Then vibration and acoustic response studies are carried out at different intensities of the VAL by considering the pre-stress effect. An isotropic beam made of aluminium with cross section $b \times h$ and length $L = 1$ m is used in the study. The beam is having square cross section and aspect ratio $L/h = 50$ defines thickness of the beam and $E = 70$ GPa; $\nu = 0.3$; $\rho = 2700\ \mathrm{kg/m^3}$ are its material properties. The six variants of the VALs (Fig. 2) are obtained by changing the coefficients β_1, β_2, and β_3 in Eq. (1) as given in Table 1.

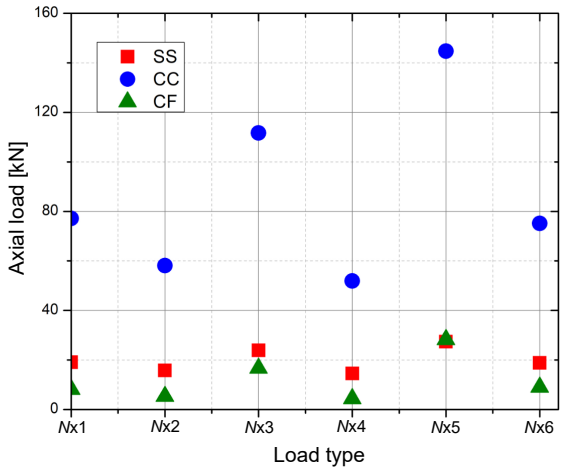

Fig. 4. Variation in buckling loads for the three boundary conditions under various VALs.

4.1. Buckling behaviour

Figure 4 depicts the effect on critical buckling loads with change in boundary conditions and VALs. As anticipated stiffness of the beams is influencing the buckling strength. The difference between the critical buckling load values of SS and CF beams is marginal comparing with SS beams having higher magnitudes than CF beams except for N_x^5 loading. The trend in the variation of critical buckling loads across VALs is the same for all the three boundary conditions and is also depicting the same as earlier studies of Karamanli and Aydogdu (2019a) as well. The lowest and highest values in buckling load across each boundary condition is reporting to be for N_x^4 and N_x^5 axial loads, respectively. In comparison to uniformly distributed load N_x^1, the bell shaped (N_x^6) axially variable in-plane load is having lower critical buckling load value. From Fig. 4 it is evident that N_x^3 and N_x^5 load distributions report higher critical buckling loads, and N_x^2, N_x^4, and N_x^6 loads reporting relatively lower critical buckling loads. Hence, the nature of variation of VAL highly influences the buckling behaviour of the beam. N_x^4 loading is considered for case 2 studies as the least critical buckling load is observed for this loading. Influence of nature of variation of VAL on the fundamental buckling mode shapes of the beam under different boundary conditions is not much seen as shown in Fig. 5.

4.2. Free vibration frequency

Free vibration and acoustic response studies are carried out at different magnitudes of the axial load for the given type of VAL. This study is done in two different ways:

(i) Case 1: the magnitude of the applied load is changed according to buckling load associated with the corresponding VAL load.

(ii) Case 2: the applied load is changed according to least critical buckling load out of all the VALs.

The case studies on the effect of varying critical buckling loads on natural frequency for the three different boundary conditions are plotted in Figs 6–8. Each figure consists of two case study plots, variation of fundamental frequency under case 1 loading as shown in plot (a), and variation of fundamental frequency under case 2 loading as shown in plot (b).

Plots in Fig. 6 present the effect on the fundamental frequency of SS beam due to increase in axial load intensity under different VALs. For case 1, as the respective critical buckling load of each axial load is considered for the analysis, the variation of natural frequency under the given VAL is observed to be zero at their associated critical buckling load. This trend in natural frequency is also observed by other researchers in earlier studies. The difference in the trends of funda-

Table 4. Buckling loads for various VALs.

BC	N_x^1	N_x^2	N_x^3	N_x^4	N_x^5	N_x^6
SS	19050.38	15751.79	23842.64	14522.32	27368.42	18821.46
CC	77144.71	58115.54	111650.02	51881.54	144745.89	75190.83
CF	8083.92	5279.79	16639.04	4350.24	28221.40	8990.26

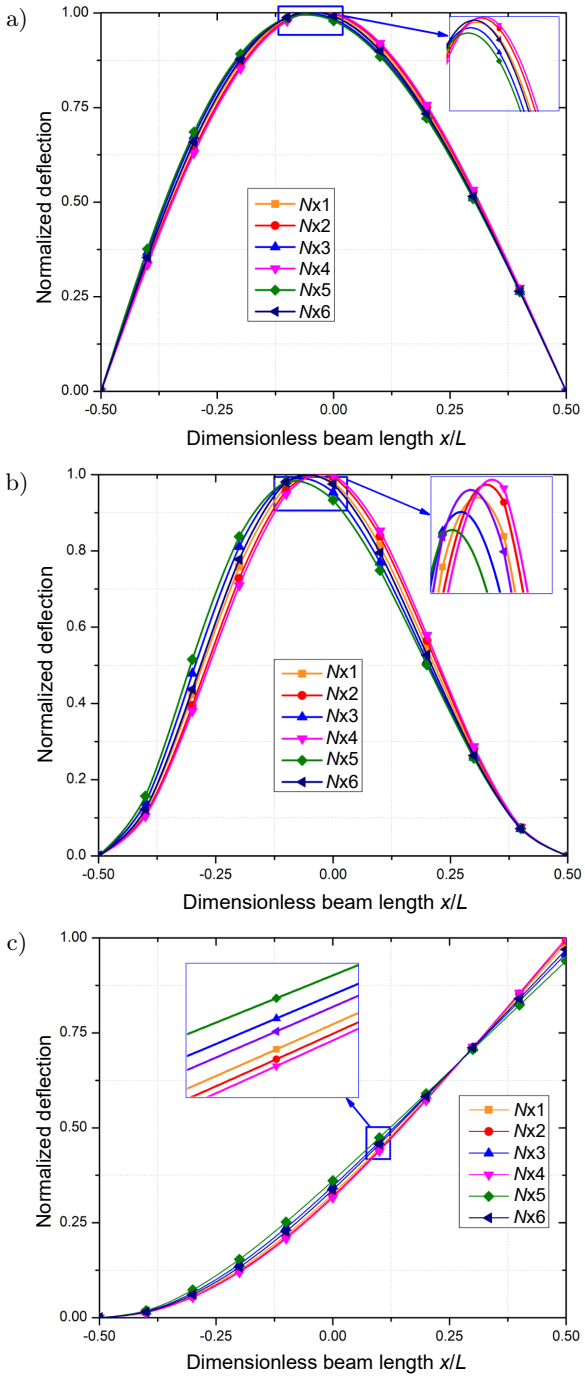

Fig. 5. Effect of nature of VAL on fundamental buckling mode shape of various beams: a) SS, b) CC, c) CF.

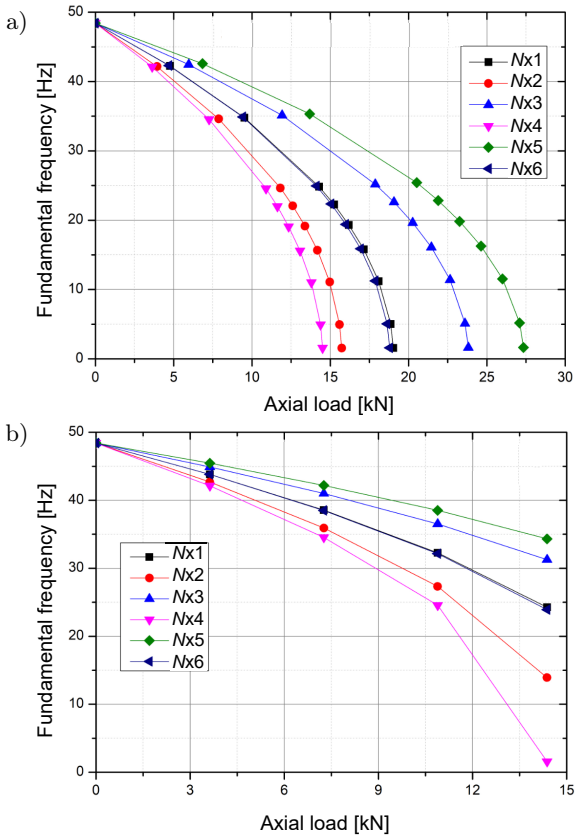

Fig. 6. Influence of increase in axial load on the fundamental frequency of SS beam: a) case 1, b) case 2.

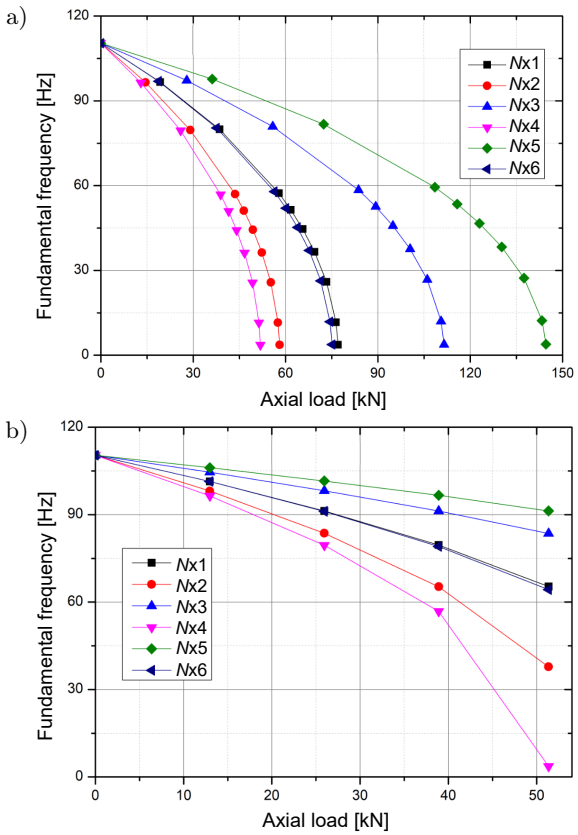

Fig. 7. Influence of increase in axial load on the fundamental frequency of CC beam: a) case 1, b) case 2.

mental frequency for the two cases can be easily depicted from Fig. 6. As Fig. 6b is plotted by taking P_{cr} of N_x^4 load, its corresponding fundamental frequency is observed to be zero at the P_{cr} and for the remaining load cases the natural frequencies are following a reducing trend with increase in the load without approaching to zero. The similar variation in natural frequency is observed for higher modes also. Variation in natural frequency with rise in axial load is similar to all the three beams as shown in Figs 7 and 8. Simi-

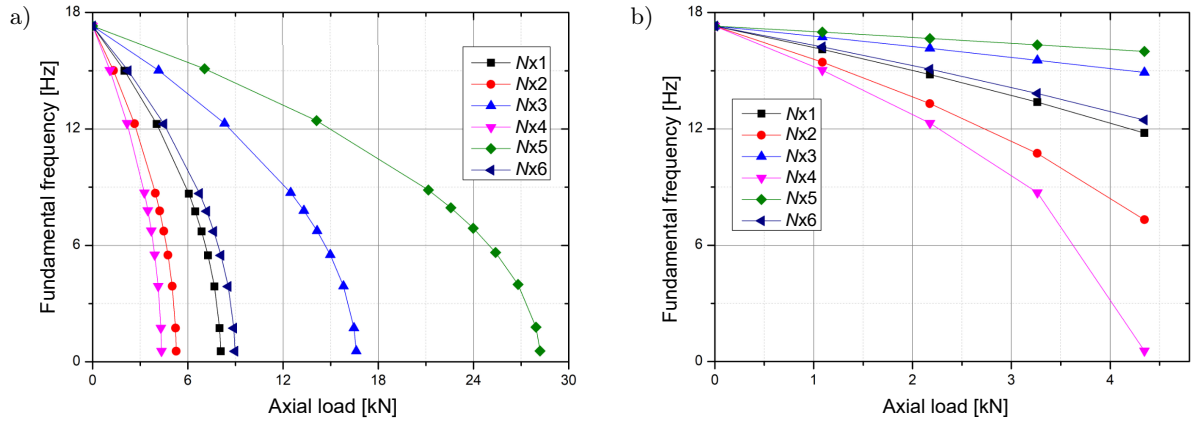

Fig. 8. Influence of increase in axial load on the fundamental frequency of CF beam: a) case 1, b) case 2.

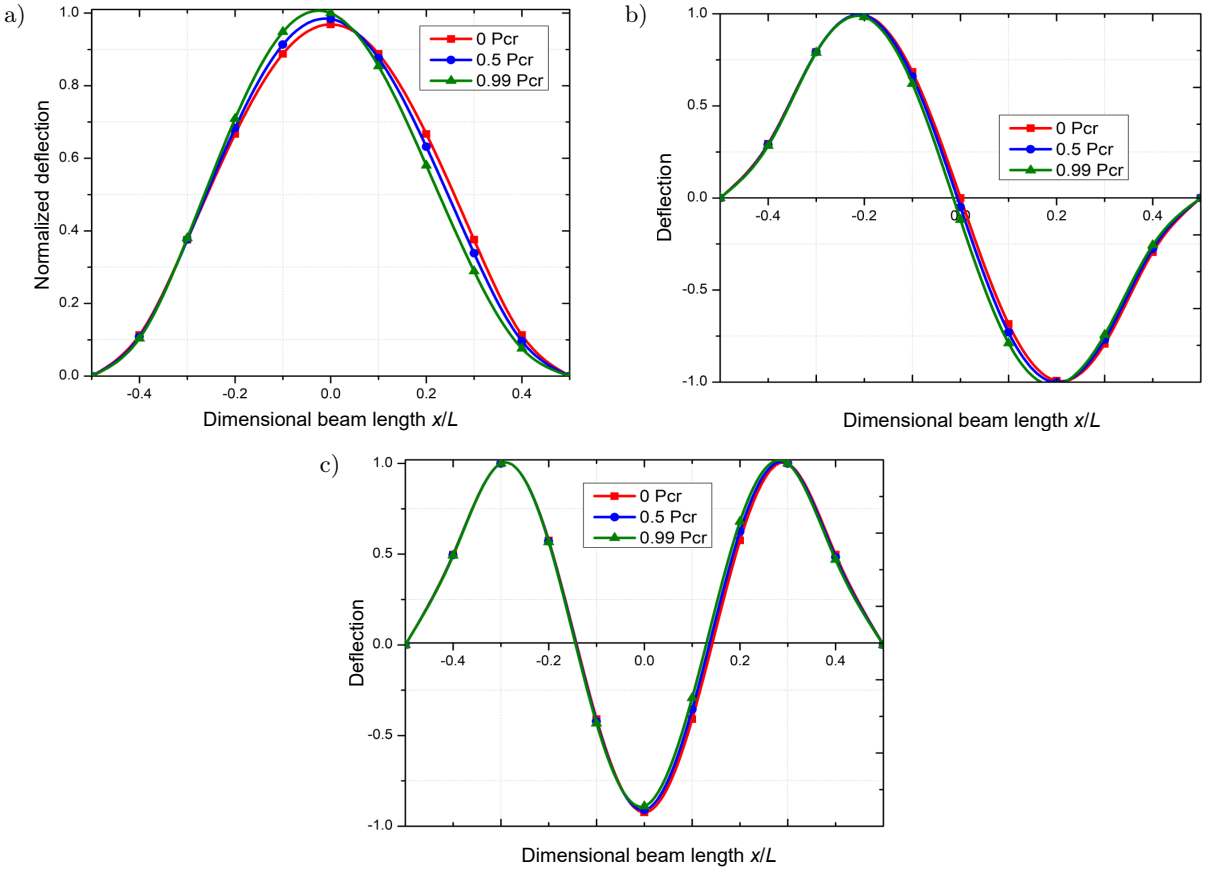

Fig. 9. Influence of increase in axial load intensity on free vibration modes of CC beams under N_x^4 loading: a) 1st mode, b) 2nd mode, c) 3rd mode.

larly, influence of type of VAL on fundamental mode of CC beam subjected to N_x^4 load case is presented in Fig. 9. The plots in Fig. 9 depict marginal variation across the first three mode shapes with variation in axial compression load.

4.3. Acoustic response

Effect of variation in VAL on acoustic response characteristics is investigated in this section. The beam is excited with 1 N of harmonic force in 0 to 1500 Hz frequency range. The acoustic response analysis in the present study is carried for the least critical buckling load (P_{cr}), which is observed for N_x^4 axial load. The effect of variation in VAL is determined by considering respective loadings in fraction of $0P_{cr}$, $0.5P_{cr}$, and $0.99P_{cr}$. The beam is excited at 0.7 m form the left extreme end of the beam so that the response of first few modes can be analysed.

The sound power level of the SS, CC, and CF beams under N_x^4 and N_x^5 cases at different intensities of applied load, in terms of fractions of P_{cr} of the

corresponding load case, is shown in Fig. 10. Due to the reduction in beam stiffness with rise in magnitude of applied load, there is a decrease in natural frequencies of each mode. This shift in natural frequencies can be clearly seen for the CC beam compared to the other cases. Similarly, in most of the cases the resonant amplitudes of each mode reduces with rise in magnitude of VAL. This trend can be clearly seen for the peak amplitudes of the fundamental mode. Basically, the reduction in beam stiffness should lead to increase in response amplitudes, but reverse trend is observed here. The sound power is a function of normal velocity which is a function of displacement amplitude and frequency. The reduction in natural

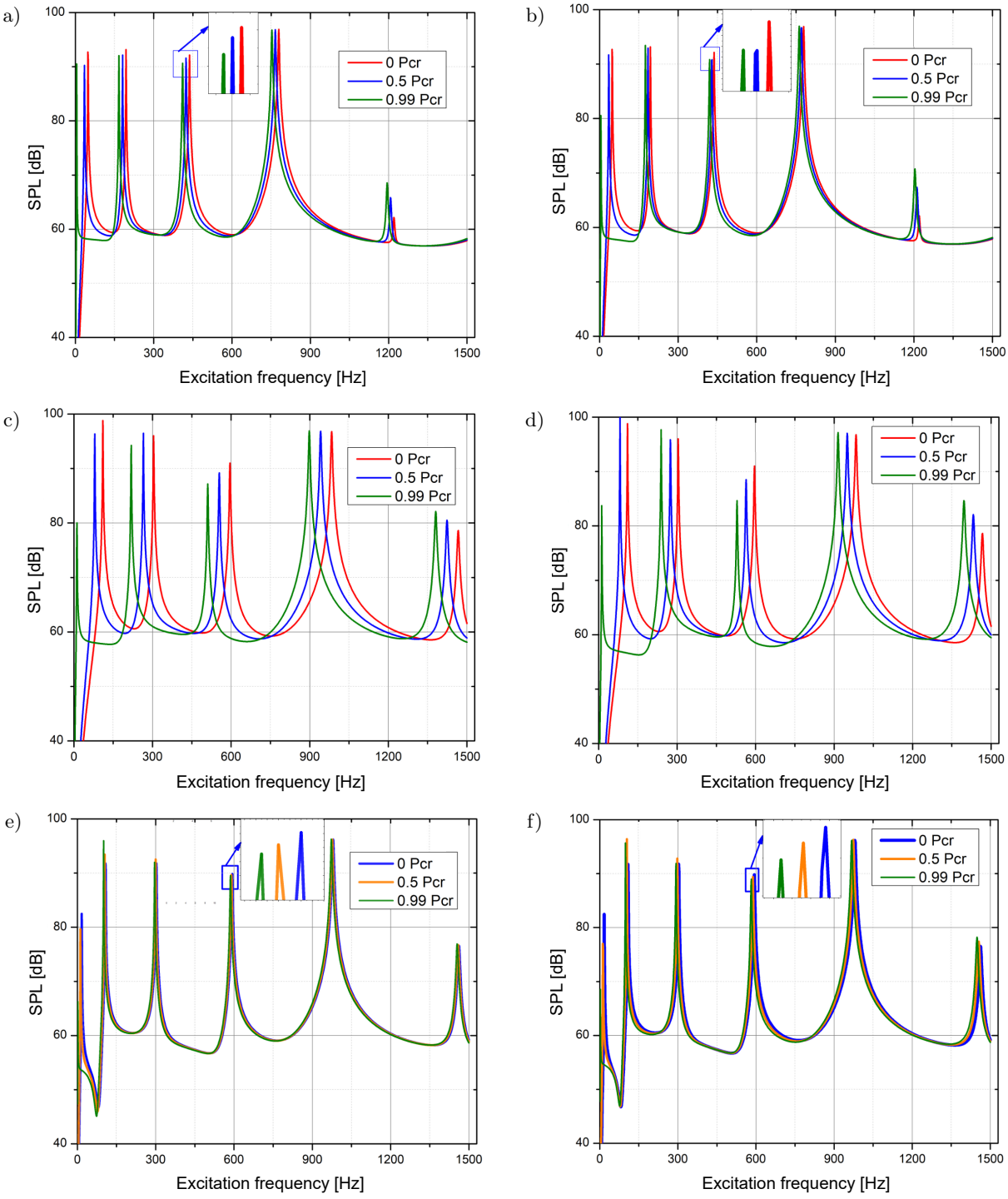

Fig. 10. Effect of magnitude of VAL on sound power response: a) SS beam under N_x^4 loading, b) SS beam under N_x^5 loading, c) CC beam under N_x^4 loading, d) CC beam under N_x^5 loading, e) CF beam under N_x^4 loading, f) CF beam under N_x^5 loading.

frequency in turn reduced the velocity and sound, which resulted in reduction of sound power radiated. However, the trend in variation of resonant amplitudes with rise in magnitude of VAL is reverse for the fifth mode which can be clearly seen for the CC beam. The shift in natural frequencies and variation in peaks with rise in the intensity of applied VAL are not clearly seen for SS beams (Figs 10a and 10b) and CF beams (Figs 10e and 10f). However, the variations in natural frequency and peaks are similar to the CC beams as seen in the sub-figures. The variation seems to be insignificant in the actual figure due to very low stiffness associated with the SS and CF beams. The resonant amplitude increases with rise in magnitude of the load for the fifth mode. Influence of rise in magnitude of the load and boundary condition is negligible on sound radiation efficiency of the beams as shown in Fig. 11. This indicates that the radiation efficiency is not sensitive to increase in axial load intensity. The results of SS, CC, and CF beams under N_x^4 loading of Fig. 10 are presented as constant octave bands in Fig. 12. Figure 12 charts depicts the effect of increase in axial load is following nonuniformity trend for increase in octave band frequencies.

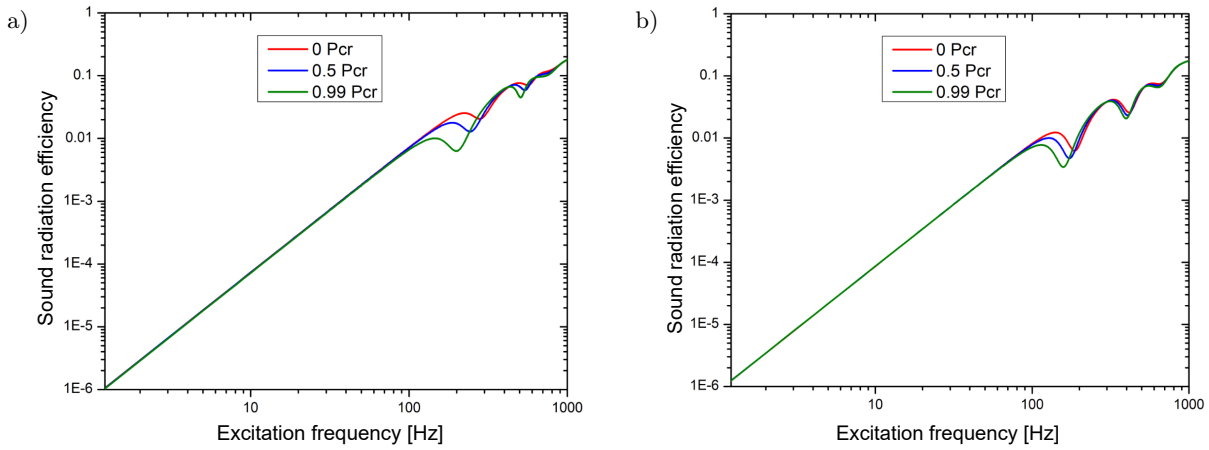

Fig. 11. Effect of magnitude of VAL on sound radiation efficiency: a) SS beam under N_x^4 loading, b) CC beam under N_x^4 loading.

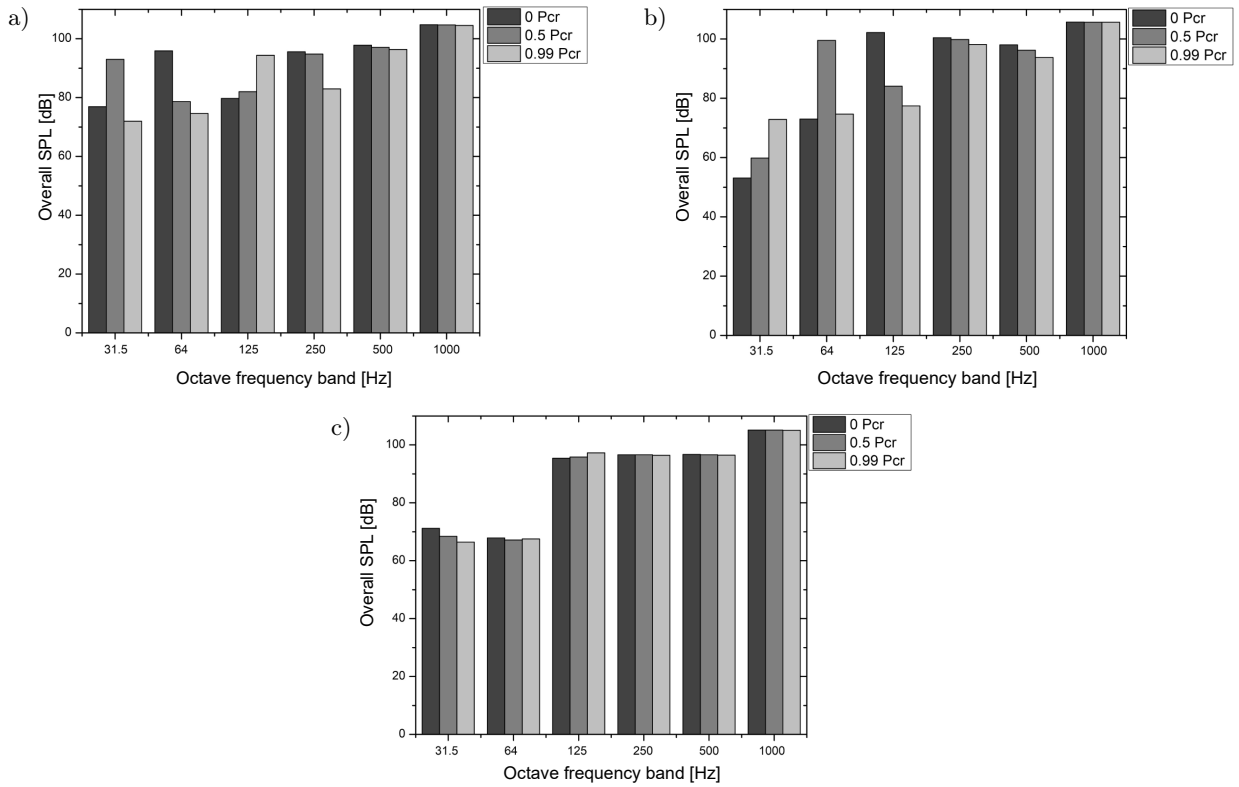

Fig. 12. Effect of magnitude of VAL on overall sound power level: a) SS beam under N_x^4 loading, b) CC beam under N_x^5 loading, c) CF beam under N_x^5 loading.

Increase in the amplitude is due to the association of natural frequency in that respective loading fraction. From the charts it is evident that more the stiffness of the beam more will be the variation in the natural frequency and more is the variation in the SWL in the octave bands. The overall SWL for increase in loading fraction for SS, CC, and CF beams is plotted in Fig. 13. Figure 13 depicts that with increase in axial load there is decreasing in the overall SWL amplitudes for SS and CC beams. For CF beams the trend is uniform from $0P_{cr}$ to $0.5P_{cr}$ axial load and marginally increasing from $0.5P_{cr}$ to $0.99P_{cr}$ axial load.

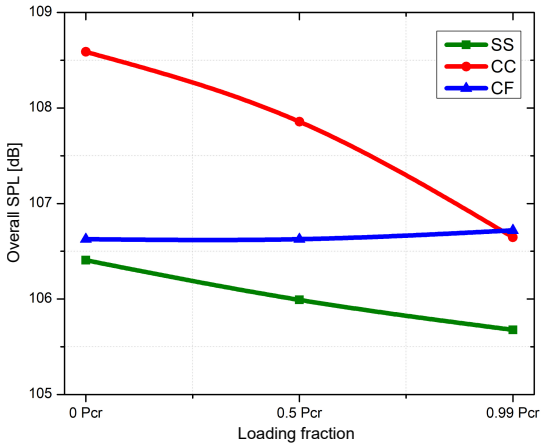

Fig. 13. Effect of increasing VAL on overall sound power.

The sound pressure level (SPL) radiated from the beams is represented as contour plot in Table 5 upto a distance of 1.5 m above the beam. Contour plots shown in Table 5 are plotted at fundamental frequency across the distances along length and thickness directions of the beam. Graphs in Table 5 are plotted for fundamental mode of SS and CF beams for increase in loading fraction. Similarly, contour plots for fundamental mode of CC beams are represented in Table 6. As anticipated the structural stiffness effected the SPL, which is observed to be more for CC beams than compared to SS and CF beams. The shift of sound radiation in CF beams is due to the variation in edge stiffness of the beam. For SS and CC beams sound radiation is observed to be concentric from center due to their equal edge stiffness. Effect of loading fraction on SPL is found to be less significant on all the three beams for their fundamental frequencies. From the plots it is evident that with increase in compression load there is marginal decrement in intensity of sound radiation. The marginal decrement is reporting to be of the same trend of SWL plotted in Fig. 10. To have better understanding in the behaviour of the beams for higher order modes, CC beams under N_x^4 axial loading is analysed for varying loading fraction. From the 5th modal frequency trends of Table 6 contour plots and Fig. 10 SWL plots, it is evident that with increase in axial compression load there is increase in sound radiation. The SPL directivity pattern at a distance of 1.0 m from the beam is studied for the three beams and is presented in Fig. 14. Figures 14a, 14c, and 14e are plotted for fundamental mode of SS, CC, and CF beams for increase in axial compression

Table 5. Contour representation effect of increasing axial load sound pressure level radiated.

BC	$0P_{cr}$	$0.5P_{cr}$	$0.99P_{cr}$
SS	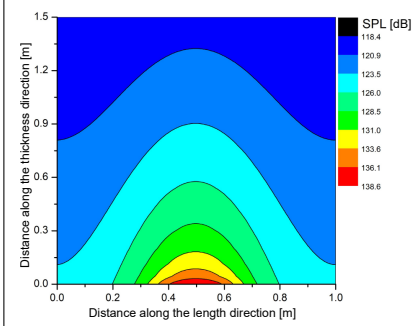	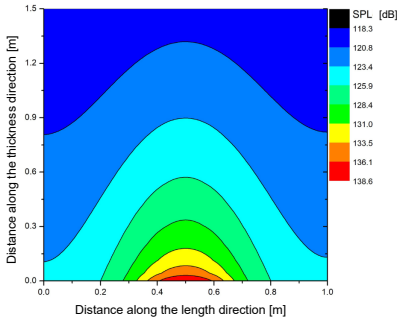	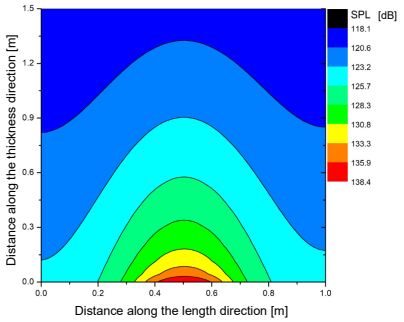
CF	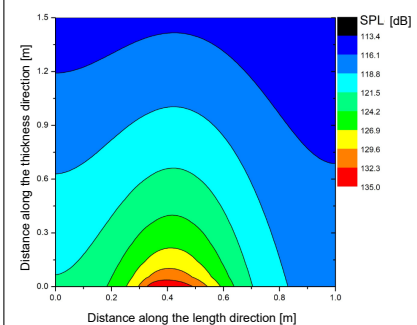	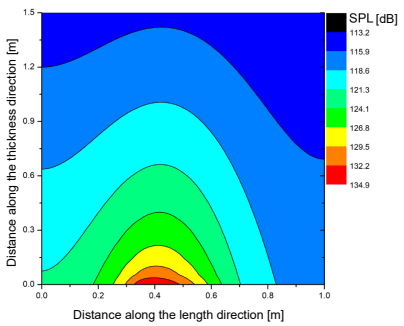	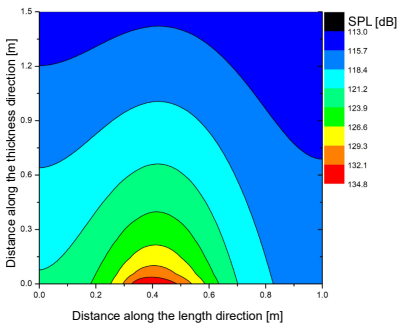

Table 6. Contour representation effect of increasing axial load sound pressure level radiated for CC beam.

BC	$0P_{cr}$	$0.5P_{cr}$	$0.99P_{cr}$
1st	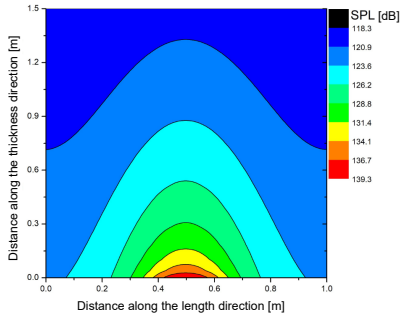	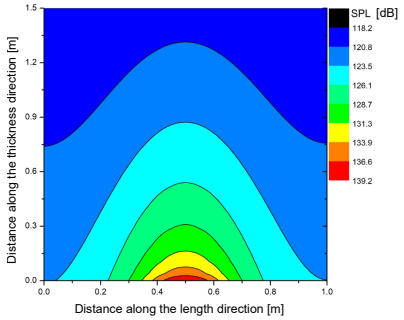	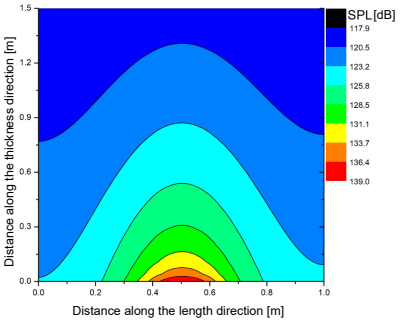
5th	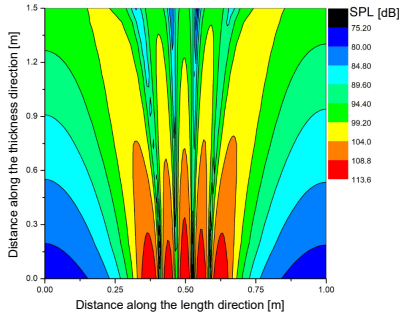	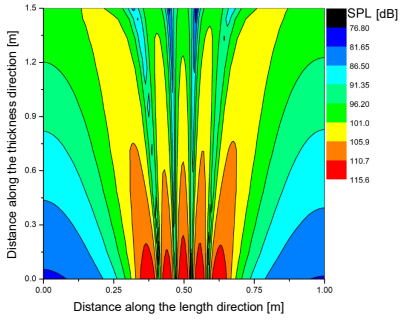	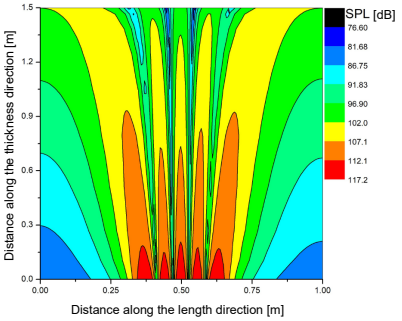

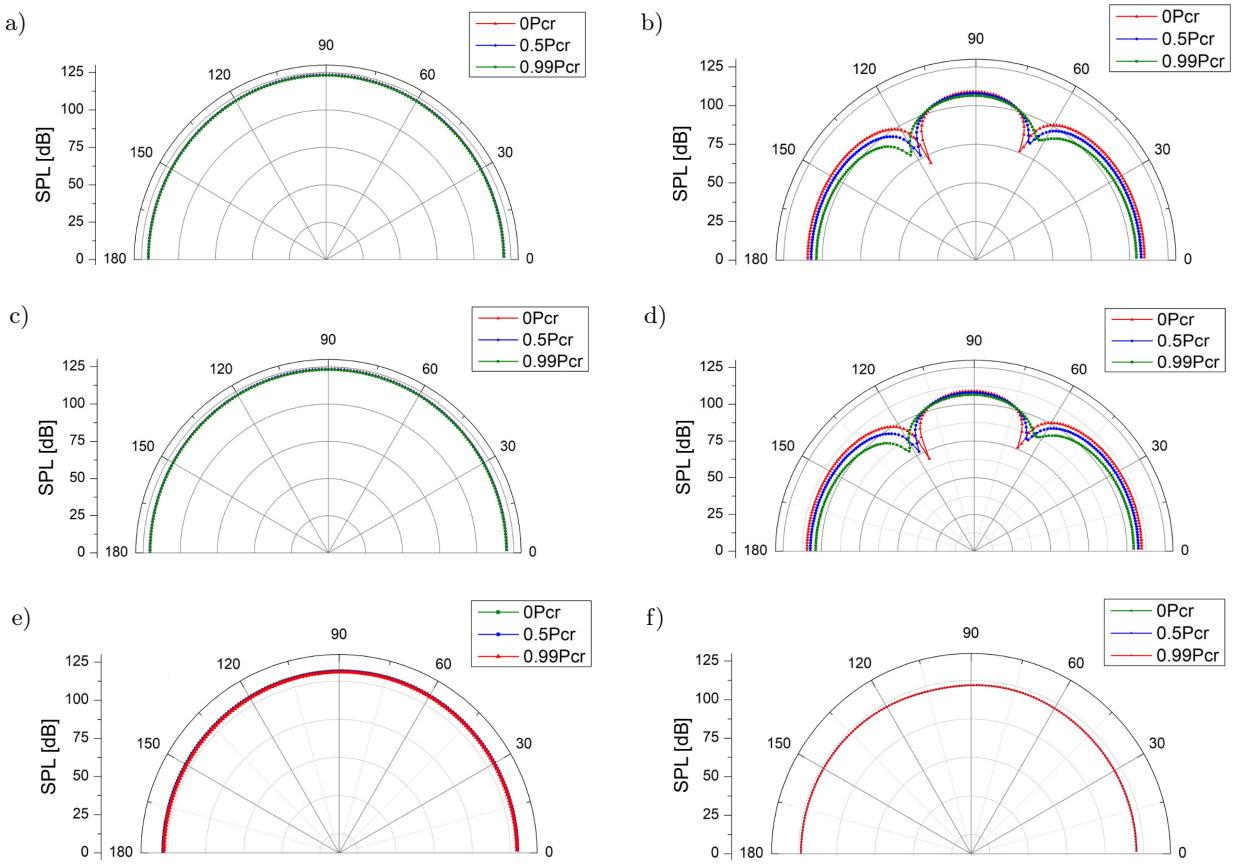

Fig. 14. Effect of increase in VAL on directivity pattern: a) for SS beam under N_x^4 loading, b) third mode of SS beam under N_x^4 loading, c) for CC beam under N_x^4 loading, d) third mode of CC beam under N_x^4 loading, e) for CF beam under N_x^4 loading, f) third mode of CF beam under N_x^4 loading.

load. The variation in SPL with increase in loading fraction is marginal for the fundamental mode of the three beams. From these plots it is evident that with increase in axial compression load the SPL is partially reducing. The plots in Figs 14b, 14d, and 14f depict the effect of loading fraction on third mode. The effect of loading fraction in directivity pattern is more significant in third modes of SS and CC beams compared to CF beams.

5. Conclusion

Aluminium beam is investigated for vibro-acoustic response for the six different types of VALs and for three boundary conditions SS, CC, and CF. Variation in buckling and free vibration characteristics under the different VALs also analysed. From the study the following conclusions are drawn:

- Critical buckling loads are sensitive to nature of variation of VAL and boundary conditions.
- Rise in the intensity of VAL leads to significant reduction in natural frequencies and the fundamental frequency approaches zero when the magnitude of the applied load is equal to buckling load.
- Sound power resonant values are influenced by the intensity of VAL and the variation in the resonant amplitude is clearly seen for the CC beam compared to the SS and CF beams.
- Significant changes in sound power level are seen in lower frequency bands while there is not much variation in overall sound power level with variation in magnitude of the applied VAL.

Appendix

$$K_{11}(i,j) = A\int_{-\frac{L}{2}}^{\frac{L}{2}} \Theta_{i,x}\Theta_{j,x}\,\mathrm{d}x,$$

$$K_{12}(i,j) = -B\int_{-\frac{L}{2}}^{\frac{L}{2}} \Theta_{i,x}\varphi_{j,xx}\,\mathrm{d}x,$$

$$K_{13}(i,j) = -B_s\int_{-\frac{L}{2}}^{\frac{L}{2}} \Theta_{i,x}\zeta_{j,xx}\,\mathrm{d}x,$$

$$K_{14}(i,j) = X\int_{-\frac{L}{2}}^{\frac{L}{2}} \Theta_{i,x}\psi_j\,\mathrm{d}x,$$

$$K_{22}(i,j) = D\int_{-\frac{L}{2}}^{\frac{L}{2}} \varphi_{i,xx}\varphi_{j,xx}\,\mathrm{d}x,$$

$$K_{23}(i,j) = H\int_{-\frac{L}{2}}^{\frac{L}{2}} \varphi_{i,xx}\zeta_{j,xx}\,\mathrm{d}x,$$

$$K_{24}(i,j) = -Y\int_{-\frac{L}{2}}^{\frac{L}{2}} \varphi_{i,xx}\psi_j\,\mathrm{d}x,$$

$$K_{33}(i,j) = D_s\int_{-\frac{L}{2}}^{\frac{L}{2}} \zeta_{i,xx}\zeta_{j,xx}\,\mathrm{d}x + A_s\int_{-\frac{L}{2}}^{\frac{L}{2}} \zeta_{i,x}\zeta_{j,x}\,\mathrm{d}x,$$

$$K_{34}(i,j) = -Y_s\int_{-\frac{L}{2}}^{\frac{L}{2}} \zeta_{i,xx}\psi_j\,\mathrm{d}x + A_s\int_{-\frac{L}{2}}^{\frac{L}{2}} \zeta_{i,x}\psi_{j,x}\,\mathrm{d}x,$$

$$K_{44}(i,j) = Z\int_{-\frac{L}{2}}^{\frac{L}{2}} \zeta_i\zeta_j\,\mathrm{d}x + A_s\int_{-\frac{L}{2}}^{\frac{L}{2}} \zeta_{i,x}\zeta_{j,x}\,\mathrm{d}x,$$

$$S_{22}(i,j) = \int_{-\frac{L}{2}}^{\frac{L}{2}} P(x)\left(\int_{-\frac{L}{2}}^{x} \varphi_{i,x}\varphi_{j,x}\,\mathrm{d}x\right)\mathrm{d}x,$$

$$S_{23}(i,j) = \int_{-\frac{L}{2}}^{\frac{L}{2}} P(x)\left(\int_{-\frac{L}{2}}^{x} \varphi_{i,x}\zeta_{j,x}\,\mathrm{d}x\right)\mathrm{d}x,$$

$$S_{24}(i,j) = \int_{-\frac{L}{2}}^{\frac{L}{2}} P(x)\left(\int_{-\frac{L}{2}}^{x} \zeta_{i,x}\zeta_{j,x}\,\mathrm{d}x\right)\mathrm{d}x,$$

$$M_{11}(i,j) = \int_{-\frac{L}{2}}^{\frac{L}{2}} m_0\Theta_i\Theta_j\,\mathrm{d}x,$$

$$M_{12}(i,j) = -\int_{-\frac{L}{2}}^{\frac{L}{2}} m_1\Theta_i\varphi_{j,x}\,\mathrm{d}x,$$

$$M_{13}(i,j) = \int_{-\frac{L}{2}}^{\frac{L}{2}} m_f\Theta_i\psi_{j,x}\,\mathrm{d}x,$$

$$M_{22}(i,j) = \int_{-\frac{L}{2}}^{\frac{L}{2}} (m_0\varphi_i\varphi_j + m_2\varphi_{i,x}\varphi_{j,x})\,\mathrm{d}x,$$

$$M_{23}(i,j) = \int_{-\frac{L}{2}}^{\frac{L}{2}} (m_0\varphi_i\zeta_j + m_{fz}\varphi_{i,x}\zeta_{j,x})\,\mathrm{d}x,$$

$$M_{24}(i,j) = \int_{-\frac{L}{2}}^{\frac{L}{2}} m_g\varphi_i\psi_j\,\mathrm{d}x,$$

$$M_{33}(i,j) = \int_{-\frac{L}{2}}^{\frac{L}{2}} (m_0 \zeta_i \zeta_j + m_{f^2} \zeta_{i,x} \zeta_{j,x}) \, \mathrm{d}x,$$

$$M_{34}(i,j) = \int_{-\frac{L}{2}}^{\frac{L}{2}} m_g \zeta_i \psi_j \, \mathrm{d}x,$$

$$M_{44}(i,j) = \int_{-\frac{L}{2}}^{\frac{L}{2}} m_{g^2} \psi_i \psi_j \, \mathrm{d}x.$$

References

1. Abo-bakr R.M., Abo-bakr H.M., Mohamed S.A., Eltaher M.A. (2021), Optimal weight for buckling of FG beam under variable axial load using Pareto optimality, *Composite Structures*, **258**: 113193, doi: 10.1016/j.compstruct.2020.113193.
2. Alshabatat N.T., Naghshineh K. (2014), Optimization of natural frequencies and sound power of beams using functionally graded material, *Advances in Acoustics and Vibration*, **2014**: Article ID 752361, doi: 10.1155/2014/752361.
3. Aydogdu M. (2005), Vibration analysis of cross-ply laminated beams with general boundary conditions by Ritz method, *International Journal of Mechanical Sciences*, **47**(11): 1740–1755, doi: 10.1016/j.ijmecsci.2005.06.010.
4. Aydogdu M. (2006), Buckling analysis of cross-ply laminated beams with general boundary conditions by Ritz method, *Composites Science and Technology*, **66**(10): 1248–1255, doi: 10.1016/j.compscitech.2005.10.029.
5. Chakraverty S., Behera L. (2015), Free vibration of non-uniform nanobeams using Rayleigh-Ritz method, *Physica E: Low-Dimensional Systems and Nanostructures*, **67**: 38–46, doi: 10.1016/j.physe.2014.10.039.
6. Denli H., Sun J.Q. (2007), Structural-acoustic optimization of sandwich structures with cellular cores for minimum sound radiation, *Journal of Sound and Vibration*, **301**(1–2): 93–105, doi: 10.1016/j.jsv.2006.09.025.
7. Eltaher M.A., Mohamed S.A. (2020a), Buckling and stability analysis of sandwich beams subjected to varying axial loads, *Steel and Composite Structures*, **34**(2): 241–260, doi: 10.12989/scs.2020.34.2.241.
8. Eltaher M.A., Mohamed S.A., Melaibari A. (2020b), Static stability of a unified composite beams under varying axial loads, *Thin-Walled Structures*, **147**: 106488, doi: 10.1016/j.tws.2019.106488.
9. Ghannadpour S.A., Mohammadi B., Fazilati J. (2013), Bending, buckling and vibration problems of nonlocal Euler beams using Ritz method, *Composite Structures*, **96**: 584–589, doi: 10.1016/j.compstruct.2012.08.024.
10. Gunasekaran V., Pitchaimani J., Chinnapandi L.B.M. (2020a), Vibro-acoustics response of an isotropic plate under non-uniform edge loading: an analytical investigation, *Aerospace Science and Technology*, **105**: 106052, doi: 10.1016/j.ast.2020.106052.
11. Gunasekaran V., Pitchaimani J., Chinnapandi L.B.M., Kumar A. (2020b), Analytical solution for sound radiation characteristics of graphene nanocomposites plate: Effect of porosity and variable edge load, *International Journal of Structural Stability and Dynamics*, **21**(06): 2150087, doi: 10.1142/S0219455421500875.
12. Gunasekaran V., Pitchaimani J., Chinnapandi L.B.M. (2021), Acoustic radiation and transmission loss of FG-Graphene composite plate under nonuniform edge loading, *European Journal of Mechanics-A/Solids*, **88**: 104249, doi: 10.1016/j.euromechsol.2021.104249.
13. Hamed M.A., Mohamed S.A., Eltaher M.A. (2020a), Buckling analysis of sandwich beam rested on elastic foundation and subjected to varying axial in-plane loads, *Steel and Composite Structures*, **34**(1): 75–89, doi: 10.12989/scs.2020.34.1.075.
14. Hamed M.A., Abo-bakr R.M., Mohamed S.A., Eltaher M.A.(2020b), Influence of axial load function and optimization on static stability of sandwich functionally graded beams with porous core, *Engineering with Computers*, **36**(4): 1929-1946, doi: 10.1007/s00366-020-01023-w.
15. Harsha B., Jeyaraj P., Lenin B. (2021), Effect of porosity and profile axial loading on elastic buckling and free vibration of functionally graded porous beam, [in:] *IOP Conference Series: Materials Science and Engineering*, **1128**: 012025, IOP Publishing, doi: 10.1088/1757-899X/1128/1/012025.
16. Hu H., Badir A., Abatan A. (2003), Buckling behaviour of a graphite/epoxy composite plate under parabolic variation of axial loads, *International Journal of Mechanical Sciences*, **45**(6–7): 1135–1147, doi: 10.1016/j.ijmecsci.2003.08.003.
17. Ilanko S., Monterrubio L., Mochida Y. (2014), *The Rayleigh-Ritz Method for Structural Analysis*, John Wiley & Sons.
18. Jaworski J.W., Dowell E.H. (2008), Free vibration of a cantilevered beam with multiple steps: Comparison of several theoretical methods with experiment, *Journal of Sound and Vibration*, **312**(4–5): 713–725, doi: 10.1016/j.jsv.2007.11.010.
19. Karamanli A., Aydogdu M. (2019a), Buckling of laminated composite and sandwich beams due to axially varying in-plane loads, *Composite Structures*, **210**: 391–408, doi: 10.1016/j.compstruct.2018.11.067.
20. Karamanli A., Aydogdu M. (2019b), On the vibration of size dependent rotating laminated composite and sandwich microbeams via a transverse shear-normal deformation theory, *Composite Structures*, **216**: 290–300, doi: 10.1016/j.compstruct.2019.02.044.

21. Kanade S.A., Chinnapandi L.B.M., Jeyaraj P., Subramanian J. (2021), Buckling and vibration behavior of composite beam due to axially varying in-plane loads, [in:] *IOP Conference Series: Materials Science and Engineering*, **1128**: 012043, IOP Publishing, doi: 10.1088/1757-899X/1128/1/012043.

22. Leissa A.W. (2005), The historical bases of the Rayleigh and Ritz methods, *Journal of Sound and Vibration*, **287**(4–5): 961–978, doi: 10.1016/j.jsv.004.12.021.

23. Li Q., Yang D. (2020), Vibro-acoustic performance and design of annular cellular structures with graded auxetic mechanical metamaterials, *Journal of Sound and Vibration*, **466**: 115038, doi: 10.1016/j.jsv.2019.115038.

24. Majkut L. (2006), Acoustical diagnostics of cracks in beam like structures, *Archives of Acoustics*, **31**(1): 17–28.

25. Melaibari A., Abo-bakr R.M., Mohamed S.A., Eltaher M.A. (2020b), Static stability of higher order functionally graded beam under variable axial load, *Alexandria Engineering Journal*, **59**(3): 1661–1675, doi: 10.1016/j.aej.2020.04.012.

26. Melaibari A., Khoshaim A.B., Mohamed S.A., Eltaher M.A. (2020a), Static stability and of symmetric and sigmoid functionally graded beam under variable axial load, *Steel and Composite Structures*, **35**(5): 671–685, doi: 10.12989/scs.2020.35.5.671.

27. Nguyen N.-D., Nguyen T.-K., Vo T.P., Thai H.-T. (2018), Ritz-based analytical solutions for bending, buckling and vibration behavior of laminated composite beams, *International Journal of Structural Stability and Dynamics*, **18**(11): 1850130, doi: 10.1142/S0219455418501304.

28. Omidi Soroor A., Asgari M., Haddadpour H. (2021), Effect of axially graded constraining layer on the free vibration properties of three layered sandwich beams with magnetorheological fluid core, *Composite Structures*, **255**: 112899, doi: 10.1016/j.compstruct.2020.112899.

29. Ruzzene M. (2004), Vibration and sound radiation of sandwich beams with honeycomb truss core, *Journal of Sound and Vibration*, **277**(4–5): 741–763, doi: 10.1016/j.jsv.2003.09.026.

30. Spadoni A., Ruzzene M. (2006), Structural and acoustic behavior of chiral truss-core beams, *Journal of Vibration and Acoustics, Transactions of the ASME*, **128**(5): 616–626, doi: 10.1115/1.2202161.

31. Tang H.B., Xu B.G. (2017), Vibroacoustic modeling of an elastic beam in low subsonic flows with mean velocities, *European Journal of Mechanics, A/Solids*, **66**: 322–328, doi: 10.1016/j.euromechsol.2017.08.004.

32. Tiryakioglu B. (2020), Radiation of sound waves by a semi-infinite duct with outer lining and perforated end, *Archives of Acoustics*, **45**(1): 77–84 doi: 10.24425/aoa.2020.132483.

33. Tiryakioglu B., Demir A. (2019), Sound wave radiation from partially lined duct, *Archives of Acoustics*, **44**(2): 239–249, doi: 10.24425/aoa.2019.128487.

34. Torres-Romero J., Cardenas W., Carbajo J., Segovia Eulogio E.-G., Ramis-Soriano J. (2018), An experimental approach to vibro-acoustic study of beam-type structures, *Archives of Acoustics*, **43**(2): 283–295, doi: 10.24425/122376.

35. Vo T.P., Thai H.-T., Aydogdu M. (2017), Free vibration of axially loaded composite beams using a four-unknown shear and normal deformation theory, *Composite Structures*, **178**: 406–414, doi: 10.1016/j.compstruct.2017.07.022.

36. Zheng H., Cai C. (2004), Minimization of sound radiation from based beams through optimization of partial constrained layer damping treatment, *Applied Acoustics*, **65**(5): 501–520, doi: 10.1016/j.apacoust.2003.11.008.

37. Zhu T.L. (2011), The vibrations of pre-twisted rotating Timoshenko beams by the Rayleigh-Ritz method, *Computational Mechanics*, **47**(4): 395–408, doi: 10.1007/s00466-010-0550-9.